PERGAMON

International Journal of Solids and Structures 37 (2000) 3031–3054

INTERNATIONAL JOURNAL OF SOLIDS and STRUCTURES

www.elsevier.com/locate/ijsolstr

Tubes in tubes: catheter navigation in blood vessels and its applications

W. Lawton [1], R. Raghavan*, [2], S.R. Ranjan, R.R. Viswanathan

Center for Information-enhanced Medicine, National University of Singapore, 10 Science Park Road, No. 03–14 The Alpha, Science Park II, Singapore 117684

Received 26 February 1998; in revised form 15 March 1999

Abstract

The construction of realistic simulators for medical procedures is increasingly important. We describe here a physical model and a numerical algorithm to simulate the insertion and navigation of a catheter into an arterial system. A novel formulation of the elasticity of thin rods was developed for modeling the catheter. The catheter bends and twists within the blood vessels, not simply tracking a central curve. The inner artery walls are modeled as rigid surfaces; this constraint of catheter containment within rigid walls is implemented through the use of a wall potential. The model has been integrated into an interactive system, with visualization and a direct catheter input interface (previously described), called *da Vinci* (**Vi**sual **n**avigation of **c**atheter **i**nsertion).

1. Medical simulation

The considerable advances in computer hardware that have occurred over the past decade, and which are continuing to occur, possess the potential for enormous impact on health care in general. In particular, the time is ripe for the construction of a series of advanced medical simulators for image-guided therapy in diverse areas with signifant advantages for physician training and for pre-treatment planning of surgical procedures. The modeling of realistic physical interactions between the virtual surgical tools and the virtual patient, together with the demand of real-time interaction, presents a formidable challenge in the construction of such systems.

In this paper, we shall focus on the realistic simulation of interventional radiology procedures

* Corresponding author. Tel.: +1-410-516-0498; fax: +1-410-516-6134.
E-mail address: raghu@cs.jhu.edu (R. Raghavan).
[1] Current address: Department of Mathematics, National University of Singapore, Singapore.
[2] Current address: Departments of Computer Science and Radiology, Johns Hopkins University, Baltimore, Maryland, USA.

0020-7683/00/$ - see front matter
PII: S0020-7683(99)00067-0

(see Anderson et al., 1996; Anderson and Raghavan, 1997). Typically, such a procedure is guided by a fluoroscopic imaging system. This assists the physician in the passage of catheters and therapeutic devices into the body. The procedure usually involves the insertion of a catheter or a guidewire into the patient's vascular system and manipulating (navigating) it to reach a region with pathology, where appropriate procedures are performed. Guidewires (over which catheters are slipped) are tools which are designed for easy navigation, and are used to guide catheters and reach desired vascular regions.

Therapies delivered by catheters include: dilation of blood vessels, narrowed from the accumulation of atherosclerotic plaque material, by applying air pressure using balloon catheters; support of weak blood vessels by placing metallic stents; blocking ruptured blood vessels by plugging materials that are transported through catheters; trapping blood clots by filtering devices; delivering drugs, and so on.

A procedure is ended by retraction of the catheter. Here, we will consider the simulation of the navigational aspect of the procedure, so that push/pull/twist manipulations performed by the physician at the free end of the catheter result in updated, physically realistic configurations of the catheter within the vascular walls. These configurations are interactively computed using a physical model of the artery–catheter interaction.

It must be emphasized that the physical model employed here is quite distinct from the simple tracking of the arterial centerline which some other simulation systems employ. As such, due to its physical behaviour within the artery walls, it has considerable benefits for training, pre-treatment planning and device design purposes.

The physical model is integrated within an entire interventional radiology simulation system with advanced visualization capabilities, whose layout is designed to reflect the environment of a catheter lab (see Anderson et al., 1996; Anderson and Raghavan, 1997). The majority of such procedures use X-ray fluoroscopy as the means of image-guidance. Contrast agents are injected into the bloodstream when the vasculature needs to be viewed in relation to the catheter for navigation purposes; this shows up in the fluoroscopic view for a few seconds. These liquids are subsequently washed downstream by the flow of blood. Physicians are accustomed to formulating three dimensional models of anatomical relationships in their mind based on the two dimensional X-ray image of the body and on the position of the catheter shown on such a display. While contrast agents provide a temporary 'road-map' of the catheter configuration in relation to the surrounding anatomy, the excessive use of these agents may result in hazardous reactions due to toxicity. The task of navigation demands considerable skill in video–eye–hand coordination to perform these procedures while maintaining reasonable levels of safety and success. These skills are currently learned by medical residents during the course of training, under the eye of experienced physicians. The presence of an alternative to patient contact at the early training stage is desirable, especially when only limited experience is available as for the most difficult and dangerous (to the patient) procedures. A training simulator could also be used for certification purposes.

Thus, the central simulation task addressed here is to develop real-time navigation of catheters in a 2-D image display similar to that used in a clinical setting. In the system we have developed, a catheter may be chosen by a physician from a library of catheters with different head shapes and with different material properties. The point of insertion (into the vasculature) may be chosen, and the physician can then commence the process of manipulation and navigation into the vasculature. A hardware device with an actual catheter is used as the input device for the manipulations; measurements sensed by the device are used as input to the finite element computation. The computationally updated configuration is then displayed on the screen.

The use of such a simulator as a pre-treatment planning tool is obvious when patient-specific data can be scanned in and a vascular model constructed therefrom. Such a tool significantly assists the choice of catheter, planning of the interventional procedure and so on.

A third important use of such a system is in the design of catheters and other interventional devices. Different materials and geometries for such devices can be tested for their performance on a library of pathologies on the computer in order to achieve optimal designs.

Although the physical model of the catheter may be constructed from standard beam elements (see, e.g. Rao, 1989), we claim several useful and new developments in this paper. First, our formulation of thin rod elasticity in Appendix A is simpler and more direct than previous descriptions (see Simo, 1985; Simo and Vu-Quoc, 1986; Love, 1944), in particular for the case considered here, namely curves that twist and bend considerably but do not stretch[3]. Secondly, we believe our formulation of finite elements Section 4 with the use of transfer matrices to relate strain increments to nodal position and orientation increments is significantly cleaner and clearer than other treatments we have encountered[4]. In formulating the constraint of containing the catheters within the arterial tubes, we use a potential function approach Section 3 is new at least in this context. We also use a fully implicit Newton's method to find the energy minimum Section 5, in contrast to more conventional semi-implicit approaches which introduce a *force* to push an object back into its constraining volume (here, a catheter into an artery). Such methods typically tend to be numerically considerably more unstable than the second order Newton method which directly finds the minimum of a quadratic form, rather than descend towards it. Our potential function method is required because the treatment of the highly non-linear constraint problem represented by two contacting non-straight tubes, one inside the other, is computationally very unwieldy. Consequently, we compute contact for the *linearized* constraint, and then use the potential function to refine this estimate. This is computationally far more efficient.

In the interactive *da Vinci* system that has been developed, we have had to compromise on several points; in particular, to make the system fully interactive without resorting to very expensive hardware, the system models fully only the head portion of the catheter, and a certain length adjacent to it. Nevertheless, at the expense of some computer time, we have constructed for the first time a full and accurate physical model of catheter and guidewire insertion and navigation. This model is described in this paper.

2. Computational model: an overview

During a catheterization procedure, the surgeon guides a guidewire through the patient's arterial system to a desired position by inserting, retracting, and turning it at the point of insertion. The catheter is then slipped over the guidewire until it reaches a desired location and used to perform various procedures there (e.g., balloon angioplasty, stent insertion, and so on). Although the movements of the catheter/guidewire system which we shall hereafter call a catheter, without, we hope, too much risk of confusion, and the arteries it contacts, are governed by dynamical laws that are computationally too complex to model exactly, these movements can be approximated simply because:

- the mass, speed and acceleration of the catheter are so small compared to the viscous forces that inertial forces are effectively dampened *instantaneously* with respect to the movement of the catheter (Important exceptions occur in thrombolysis and with microcatheters. These exceptions are not treated in this paper).

[3] The classical treatment of Love (1944), of course, is in the form of differential equations. To compare his as well as others' continuum formulation with ours, see Lawton et al. (1999).

[4] A comparison of our treatment with other computational models such as that of Simo and Vu-Quoc (1986), for instance our Eqs. (17)–(21) with the much heavier machinery of the treatment in Sections 4 and 5 of Simo and Vu-Quoc (1986), will justify our claim.

- the catheter is composed of hyperelastic material, that is its internal energy is determined by its geometric configuration,
- the artery walls are so stiff, compared to the forces exerted on them by the catheter, that their deformations are negligible.

These three assumptions imply the configuration of the inserted portion of the catheter throughout the catheterization procedure is an *equilibrium configuration* for the elastic energy subject to the following constraints:

- the *insertion point* on the catheter, located at the insertion position, is known,
- the *direction* of insertion at this insertion point as well as the rotational *orientation* of the catheter there are known,
- the inserted portion of the catheter lies within the arterial walls.

An equilibrium configuration with respect to these constraints is one that does not have arbitrarily close configurations satisfying the constraints and having less elastic energy.

Bifurcation theory arguments show that equilibrium positions are generally local energy minima and can therefore be computed by minimizing energy as the first two *insertion constraints* above are incrementally varied and the third *wall constraint* is held fixed (Lawton et al., 1997). These insertion constraints can therefore be regarded as control parameters whose trajectories are used to guide the trajectory of the catheter's configuration.

As we have stated earlier, since the walls are not planar, the wall constraint is nonlinear and exceedingly difficult to enforce directly. We chose to implement the wall constraint through the use of a *wall potential* whose effect is to provide a strong force density along any section of the inserted portion of the catheter that lies outside the inner arterial wall. This wall force acts so as to push the catheter 'back inside' the artery.

These informal arguments justify the following formulation of the catheter navigation problem (see Lawton et al., 1997 for a treatment of a class of similar variational problems): compute the deformation of a catheter, modeled as a thin rod having reference curve $\mathbf{p}_0(s)$, where s measures arc length along the catheter as it is inserted into an artery. Here, the deformation (Lawton et al., 1999) is described as follows.

The initial point on the catheter can undergo a vector displacement (translation) $\mathbf{d} \in R^3$. The catheter is described by a thin rod model with reference curve $\mathbf{p}_0$; it is assumed that the cross sections of the rod (sections perpendicular to the curve's unit tangent), upon the rod's deformation, remain perpendicular to the unit tangent of the deformed rod. With this assumption, which is equivalent to that of negligible shear of the rod's sections (Antman, 1995), the rod's deformation (and hence, elasticity) is completely described in terms of a local stretching described by a local rate of stretch α, and by its rotation action on a frame determined by the unit tangent and a single (unit) director vector perpendicular to the unit tangent (see Fig. 1). The space curve described by the catheter, together with the local frame, defines a *ribbon* familiar from differential geometry (Sternberg, 1964). This action on the frame is described by a

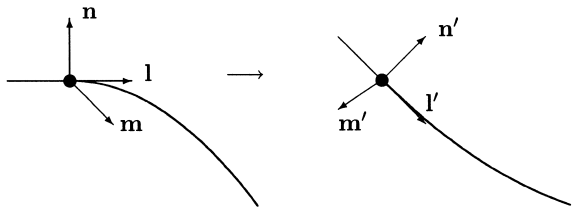

Fig. 1. A thin rod deformation showing rotation of the local frame.

three dimensional rotation which lies in the rotation group (Gilmore, 1974) in three dimensions, $SO(3)$; in general, this rotation varies along the rod. Corresponding deformations, therefore, are given by specifying the following quantities: a (rigid) translation vector $\mathbf{d}$ in three-dimensional space which gives the displacement of the initial point on the catheter; a path $g(s)$ in $SO(3)$ which describes the rotation in three dimensions of the frame at each position along the catheter; and a square integrable function $\alpha(s)$ which measures the local stretch rate at every material point on the catheter.

This description of the deformation in terms of a path in the Lie group $SO(3)$, while discussed in some other earlier treatments (Simo, 1985; Simo and Vu-Quoc, 1986), was more completely exploited in Lawton et al. (1999) and leads to elegant continuum as well as discrete formulations, ideal for computational purposes.

It is clear that the deformed curve $\mathbf{p}$ is determined by $\mathbf{p}_0$ and by the deformation $u \equiv (\mathbf{d},g,\alpha)$.

Associated with the deformed catheter is its elastic energy of deformation E_{el}. The elastic energy E_{el} which depends on the deformation u is obtained by integrating an elastic energy density Q. From invariance considerations, Q may be shown to be a function of the stretch rate α and the local pulled-back rotation *rate* (strain) $\omega(s) \equiv g^{-1}(\mathrm{d}g/\mathrm{d}s)$.

The constraint of confinement within the arterial walls is enforced by assigning a potential energy associated with the catheter exceeding its spatial bounds. The potential energy therefore depends on the space curve $\mathbf{p}(s)$ corresponding to the (deformed) current configuration of the catheter. We shall refer to this potential as the external energy; it may be written in terms of an external energy *density* $P_{\mathrm{ex}}(\mathbf{p}(s))$ defined along the catheter. The external energy density is equal to zero inside the inner artery wall and increases rapidly with outward distance from it. Since this models the interaction of the catheter with the artery wall, the total energy of the catheter–artery wall system is the sum

$$E(u) = E_{\mathrm{el}} + E_{\mathrm{ex}}, \tag{1}$$

where the respective elastic and external energies may be written as:

$$E_{\mathrm{el}} = \int_0^1 Q(\alpha(s),\omega(s))\mathrm{d}s$$

and

$$E_{\mathrm{ex}} = \int_0^1 P_{\mathrm{ex}}(\mathbf{p}(s))\mathrm{d}s. \tag{2}$$

As the catheter is inserted at the insertion point, its resulting configuration will be an equilibrium or minimum energy state of the total energy function defined above. It is clear that a sharper rise of P_{ex} beyond the artery wall corresponds to more effective confinement.

While the foregoing discussion presents a brief summary, this formulation of continuum thin rod elasticity is discussed in more detail in Appendix A, where equilibrium equations are also derived. The quadratic form (of the elastic energy density) in the rotation rate gives rise to the celebrated Kirchoff analogy with the spinning top, with the rotation rate playing the role of angular velocity of the top and arc length playing the role of time. While other formulations similar to our group-theoretic one are available (see, e.g. Simo, 1985; Simo and Vu-Quoc, 1986), we wish to call attention to the simplicity of the one given here, and in particular to the elegant form of the equilibrium equations in Appendix A. These non-linear equations lend themselves to a perturbative treatment which has an interesting analogy with time-dependent perturbation theory in quantum mechanics, discussed in detail in Lawton et al. (1999).

When the insertion of the catheter is done incrementally, given that the catheter–artery system was at

an equilibrium before an incremental insertion, the change in total energy may be written as a Taylor expansion about that equilibrium. For sufficiently small increments, the equilibrium after insertion is determined by retaining terms up to quadratic order in this expansion, and minimizing the corresponding energy. The minimization procedure is discussed in detail in Section 5. As stated earlier, this process is based on the reasonable assumption that for every incremental insertion, viscous forces which drive the catheter–artery system to an equilibrium are dominant enough that the time scale for equilibration is much smaller than the time scale required for the insertion itself.

In the next section, we shall describe details of the wall potential and the associated arterial model.

3. Arterial structure and model

3.1. Single artery wall potential

We assume the artery has a circular cross section, whose radius varies slowly. We approximate the signed distance from a point $\mathbf{p}$ on the catheter to the arterial wall by

$$d(\mathbf{p}) = |\mathbf{p} - \mathbf{q}| + R - r, \tag{3}$$

where $\mathbf{q}$ is the closest point to $\mathbf{p}$ on the central curve of the artery, R is the radius of the catheter at $\mathbf{p}$, and r is the arterial radius at $\mathbf{q}$. Note that $|\mathbf{p}-\mathbf{q}| + R - r$ is positive if and only the catheter penetrates the arterial wall and, in that case, closely approximates the extent of penetration.

We utilize a potential function P_{ex} which increases quadratically with catheter distance from the surface of the arterial tube. The potential function is thus defined by

$$P_{\text{ex}}(\mathbf{p}) := \frac{\alpha}{2} d^2 \tag{4}$$

for $d > 0$, and $P = 0$ for $d \leq 0$. Therefore

$$\nabla P_{\text{ex}}(\mathbf{p}) := \alpha d(\mathbf{p}) \frac{\mathbf{p} - \mathbf{q}}{|\mathbf{p} - \mathbf{q}|} \text{ if } d \geq 0, \text{ else: } = 0 \tag{5}$$

and

$$\text{Hessian } P_{\text{ex}}(\mathbf{p}) := \alpha \frac{d(\mathbf{p})}{|\mathbf{p} - \mathbf{q}|} I - \alpha \frac{(R - r)(\mathbf{p} - \mathbf{q})(\mathbf{p} - \mathbf{q})^T}{|\mathbf{p} - \mathbf{q}|^3}, \tag{6}$$

where I denotes the 3×3 identity matrix and $(\mathbf{p}-\mathbf{q})^T$ denotes the row vector obtained by transposing the column vector $(\mathbf{p}-\mathbf{q})$. It is clear that the potential penalizes more severely (is larger in magnitude) the further the catheter is out of the confines of the artery.

We have included here the explicit expressions for the gradient (negative force density) and Hessian of the wall potential since these quantities are needed in the determination of equilibria, as we shall discuss in the following section.

We have reduced the computation of the force density at each point $\mathbf{p}$ on the center of the catheter to the problem of computing the nearest point $\mathbf{q}$ on the central curve of the artery. We need a geometric model for the central curve and the artery wall. The inner arterial wall is constructed from the *cylindrical swept surface*, having the parameterized form

$$W_{\text{cyl}}(\mathbf{c}, r) := \left\{ \mathbf{c}(s) + r(s)\cos(\theta)\mathbf{v}(s) + r(s)\sin(\theta)\mathbf{w}(s) : s \in [0,1],\ \theta \in [0, 2\pi] \right\}, \tag{7}$$

where $\mathbf{c}$: $[0,1] \to R^3$ is a continuously differentiable function that parametrizes the center line, r:$[0,1] \to R^+$ parametrizes the radius and is less than the radius of curvature of the central curve at each point, and $\mathbf{v}$, $\mathbf{w}$:$[0,1] \to R^3$ are unit vector valued functions that are normal to the curve and to each other (see Fig. 2). This explicit parametrization of the arterial wall is specifically used for visualization. In practice $\mathbf{c}(s)$ is represented as a piecewise cubic spline function of the centerline parameter s.

We create a smooth closed surface, denoted by $W(\mathbf{c},r)$, by *capping* $W_{\text{cyl}}(\mathbf{c},r)$ at the ends with hemispherical surfaces having radii $r(0)$ and $r(1)$. Clearly, $W(\mathbf{c},r)$ is the boundary of a closed *tubular region*, denoted by $T(\mathbf{c},r)$, thus

$$W(\mathbf{c},r) = \partial T(\mathbf{c},r), \tag{8}$$

where ∂ denotes the boundary operator. For $s \in [0,1]$, let $\mathbf{t}(s)$ denote the unit tangent to the curve at $\mathbf{c}(s)$ and define the *orthogonal plane* $P(s)$ to the curve $\mathbf{c}$ at $\mathbf{c}(s)$ by

$$P(s) := \{\mathbf{q} \in R^3 : (\mathbf{q} - \mathbf{c}(s)) \cdot \mathbf{t}(s) = 0\}.$$

If $\epsilon > 0$ is sufficiently small and $\mathbf{p} \in R^3$ is ϵ close to $T(\mathbf{c},r)$, we may compute the nearest point on the centerline curve to $\mathbf{p}$, $\mathbf{q} = \mathbf{c}(s(\mathbf{p}))$, where $s(\mathbf{p}) \in [0,1]$ is the smallest value of s such that

$$|\mathbf{p} - \mathbf{c}(s(\mathbf{p}))| \le r(s(\mathbf{p})) + \epsilon \tag{9}$$

and

$$(\mathbf{p} - \mathbf{c}(s(\mathbf{p}))) \cdot \mathbf{t}(s) = 0. \tag{10}$$

Since the curve $\mathbf{c}(s)$ is represented by piecewise cubic functions in s and $\mathbf{t}(s)$ is the tangent to this curve, this last equation yields a fifth degree polynomial equation in s. It can be solved using a standard optimization method such as the Newton–Raphson method.

3.2. Multiple artery wall potential

The wall of an arterial system consisting of a collection of arteries having central curves $\mathbf{c}_n$ and radius functions r_n for $n = 1,\ldots, N$, is defined by

$$W := \partial \bigcup_{n=1}^{N} T(\mathbf{c}_n, r_n). \tag{11}$$

Elementary topology provides the following useful formula:

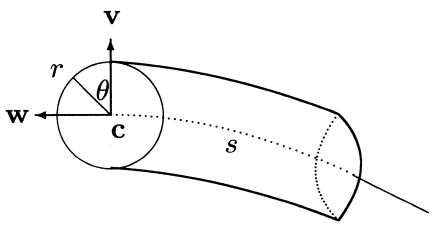

Fig. 2. The geometric artery model.

$$W = \bigcup_{n=1}^{N} \partial T(\mathbf{c}_n, r_n) \Big/ \cup_{m \neq n} T^0(\mathbf{c}_m, r_m) \tag{12}$$

where $T^0(\mathbf{c}_m, r_m)$ denotes the interior of the m-th arterial tube. These two formulae for the wall W can be used to compute whether a specified point $\mathbf{p}$ is outside W and, if so, to determine the tube it is nearest to. The potential for an arterial system is defined to be the potential for the nearest tube. The resulting potential is well-defined except along some two dimensional surfaces that are equidistant from distinct arterial branches. Possible difficulties at these places can be handled using simple heuristics.

4. Catheter model

We employ a finite element discretization to model the catheter and to compute its deformed configurations. The reference configuration of the catheter is modeled by a piecewise linear curve with nodal positions specified and the deformation is modeled by specifying displacements and orientations (described by rotation matrices) at each node. Thus, a reference (unstressed) catheter of arbitrary shape may be discretized in terms of a sequence of straight *beam elements*; successive beam elements have a single node in common. Under a deformation, the strain associated with a given beam element is quantified by its deviation from a rigid motion. It is possible to choose a sufficiently large number of elements so that the strain variables associated with each finite element are small, even when the rod as a whole undergoes large non-rigid displacements. We shall now clarify these statements.

Label the nodal points of the succession of beam elements by the index $i = 1,\ldots, n$. Consider beam $(i,i+1)$. A deformation in general changes the orientation at i by a rotation matrix M_i, and the position of i moves from $\mathbf{q}_i$ in the reference state to $\mathbf{p}_i$ in the deformed state.

We stress that the rotation effected by M_i can be a large rotation; this means that our formulation allows large shape changes (arising from large non-rigid displacements), as well as arbitrary rigid rotations of the entire rod. Suppose we pull back the position and orientation at node i (by means of a translation and a rotation) in the deformed state to match those in the unstressed state (see Fig. 3). Then the strain of element $(i,i+1)$ is quantified by the positional and orientational changes of the 'pulled back' node $(i+1)$ with respect to its position and orientation on the reference element. This is illustrated in Fig. 3 where 1–2 shows the reference element, $1'$–$2'$ the deformed element, and 1–$2''$ the deformed, pulled-back element. In this example, the pullback is effected by the inverse rotation M_1^T (the

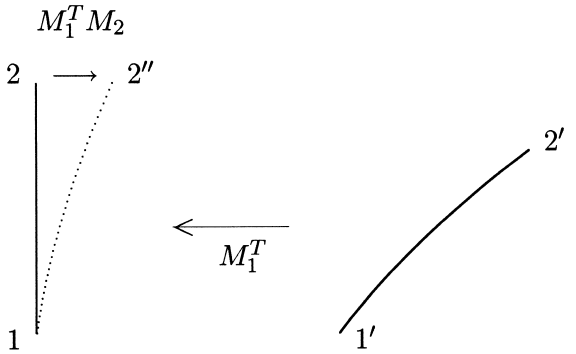

Fig. 3. Illustration of a pulled-back deformation showing the relative orientation between endpoints of the pulled back deformed element.

deformation rotates the frame at node 1 by M_1 and that at node 2 by M_2; thus M_1^T realigns the frame of the deformed element with that of the reference element at node 1). The orientation change at node $2''$ of the pulled-back element with respect to node 1 is then $M_1^T M_2$. The deviation of this relative orientation change from the identity transformation quantifies the orientational strain; similarly the positional displacement of the pulled-back node $2''$ from the reference node 2 quantifies the positional strain.

Thus, for element $(i,i+1)$, the pulled-back positional change at node $(i+1)$ is

$$\mathbf{y}_i = M_i^T(\mathbf{p}_{i+1} - \mathbf{p}_i) - (\mathbf{q}_{i+1} - \mathbf{q}_i) \tag{13}$$

and the pulled-back change in orientation between the nodes i and $i+1$ is specified by the (approximately) skewsymmetric matrix

$$\Omega_i = \left(M_i^T M_{i+1} - I\right), \tag{14}$$

where I is the 3×3 identity matrix. The variables $\mathbf{y}_i$ and Ω_i are the strain variables of element $(i,i+1)$. The (approximate) skew-symmetry of Ω_i follows from the small-strain assumption (which may be usually realized in practice by choosing sufficiently short elements) that $M_i^T M_{i+1}$ is a small rotation, and can therefore be always approximated as a skew-symmetric matrix plus the identity.

We associate to every skewsymmetric 3×3 matrix

$$\Omega = \begin{pmatrix} 0 & -\omega_3 & \omega_2 \\ \omega_3 & 0 & -\omega_1 \\ -\omega_2 & \omega_1 & 0 \end{pmatrix},$$

the vector $\boldsymbol{\omega}$ with components ω_1, ω_2 and ω_3. We shall denote by a boldface lower case letter the vector associated with the corresponding skewsymmetric matrix (denoted by the corresponding upper case letter), and vice versa.

The elastic energy associated with the strain variables $(\mathbf{y}_i,\boldsymbol{\omega}_i)$ may be expressed in terms of a 6×6 stiffness matrix K_i:

$$E_i^{\mathrm{el}} = \frac{1}{2}\left(\mathbf{y}_i^T \boldsymbol{\omega}_i^T\right) K_i \begin{pmatrix} \mathbf{y}_i \\ \boldsymbol{\omega}_i \end{pmatrix}. \tag{15}$$

The stiffness matrix K_i relates the strain to applied incremental forces. For small deformations of a rotationally symmetric element made of isotropic and homogeneous material and aligned parallel to the x-axis in its reference state, it is standard (Rao, 1989) that K_i takes the form

$$K_i = \begin{pmatrix} K_{i,1} & K^{T_{i,3}} \\ K_{i,3} & K_{i,2} \end{pmatrix}, \tag{16}$$

with the 3×3 blocks

$$K_{i,1} = \begin{pmatrix} E_Y A_i/l_i & 0 & 0 \\ 0 & 12E_Y I_i/l_i^3 & 0 \\ 0 & 0 & 12E_Y I_i/l_i^3 \end{pmatrix},$$

$$K_{i,2} = \begin{pmatrix} 2G_S I_i/l_i & 0 & 0 \\ 0 & 4E_Y I_i/l_i & 0 \\ 0 & 0 & 4E_Y I_i/l_i \end{pmatrix}$$

and

$$K_{i,3} = \begin{pmatrix} 0 & 0 & 0 \\ 0 & 0 & 6YI_i/l_i^2 \\ 0 & -6YI_i/l_i^2 & 0 \end{pmatrix}.$$

Here, A_i and I_i are the area and second moment of area of the beam element, respectively, and l_i its length. The variables E_Y and G_S are the Young's modulus and shear modulus respectively. If the element in its reference state is not aligned with the x-axis, the above form of K_i must be conjugated with an appropriate rotation matrix which aligns the beam with the x-axis.

While the form of K_i is usually obtained by considering small deformations of a straight beam, our formulation with the strain variables $\mathbf{y}_i$ and $\boldsymbol{\omega}_i$ allows us to directly use this form of the stiffness matrix; with the assumption of small strain, large shape changes (displacements) may be handled as well using our pulled-back strain variables.

The stiffness matrix may also be determined directly from integrating the perturbation equations derived in Lawton et al. (1999), for straight elements or for curved elements if needed. In the latter case the form of K_i would of course be different.

In the presence of an external potential, there is a contribution E_i^{ex} to the total energy; this term arises, as mentioned earlier, from an integration over the beam element of an external energy density.

Quasistatic equilibria may be found by a process of incremental energy minimization. To quadratic order, the incremental change in elastic energy is

$$\delta E_i^{\text{el}} = \left(\mathbf{y}_i^T \boldsymbol{\omega}_i^T\right) K_i \begin{pmatrix} \delta\mathbf{y}_i \\ \delta\boldsymbol{\omega}_i \end{pmatrix} + \frac{1}{2}\left(\delta\mathbf{y}_i^T \delta\boldsymbol{\omega}_i^T\right) K_i \begin{pmatrix} \delta\mathbf{y}_i \\ \delta\boldsymbol{\omega}_i \end{pmatrix}. \tag{17}$$

It is convenient to express the changes in the strain variables directly in terms of changes in global position and orientation in a fixed inertial frame. The changes in the strain variables, $\mathbf{y}_i$ and $\boldsymbol{\omega}_i$, may be expressed as a linear function of the changes in position $\delta\mathbf{p}_i$, $\delta\mathbf{p}_{i+1}$ and changes in orientation $\delta\boldsymbol{\phi}_i$ and $\delta\boldsymbol{\phi}_{i+1}$ through a transfer matrix D_i:

$$\begin{pmatrix} \delta\mathbf{y}_i \\ \delta\boldsymbol{\omega}_i \end{pmatrix} = D_i \begin{pmatrix} \delta\mathbf{p}_i \\ \delta\boldsymbol{\phi}_i \\ \delta\mathbf{p}_{i+1} \\ \delta\boldsymbol{\phi}_{i+1} \end{pmatrix}. \tag{18}$$

It is not hard to see that

$$D_i = \begin{pmatrix} M_i^T & 0 \\ 0 & M_i^T \end{pmatrix} \begin{pmatrix} -I & V_i & I & 0 \\ 0 & -I & 0 & I \end{pmatrix}, \tag{19}$$

with $\mathbf{v}_i = \mathbf{p}_{i+1} - \mathbf{p}_i$.

Using the quadratic expansion of the external potential energy, and making use of the assumption of small strain, the change in total energy may then be written to quadratic order as

$$\delta E_i^{\text{tot}} = -\left(L_i^{\text{el}} + L_i^{\text{ex}}\right)^T \begin{pmatrix} \delta\mathbf{p}_i \\ \delta\boldsymbol{\phi}_i \\ \delta\mathbf{p}_{i+1} \\ \delta\boldsymbol{\phi}_{i+1} \end{pmatrix} + \frac{1}{2}\left(\delta\mathbf{p}_i^T \delta\boldsymbol{\phi}_i^T \delta\mathbf{p}_{i+1}^T \delta\boldsymbol{\phi}_{i+1}^T\right)\left(K_i^{\text{ex}} + K_i^{\text{el}}\right) \begin{pmatrix} \delta\mathbf{p}_i \\ \delta\boldsymbol{\phi}_i \\ \delta\mathbf{p}_{i+1} \\ \delta\boldsymbol{\phi}_{i+1} \end{pmatrix}, \tag{20}$$

where L_i^{ex} and K_i^{ex} are the negative gradient and Hessian respectively (given in Section 3.1) of the

external potential, with respect to appropriate variables, and the elastic load vector and stiffness matrix are, respectively,

$$L_i^{\mathrm{el}} = -D_i^T K_i \begin{pmatrix} \mathbf{y}_i \\ \boldsymbol{\omega}_i \end{pmatrix} \tag{21}$$

and

$$K_i^{\mathrm{el}} = D_i^T K_i D_i. \tag{22}$$

The total energy of the system is additive over elements; minimizing δE^{tot} with suitable constraints (to account for six overall degrees of rigid motion) yields a system of linear equations for changes in position and orientation. The strain variables $\mathbf{y}_i$ and $\boldsymbol{\omega}_i$ must be kept updated throughout, and the rotation matrices are updated using $M_i \rightarrow (I + \delta\Phi_i)M_i$, where $\delta\Phi_i$ is the skewsymmetric matrix corresponding to $\delta\boldsymbol{\phi}_i$.

We note that this finite element description is directly valid for arbitrary deformations. Many existing finite element methods (Rao, 1989), on the other hand, often use iterative schemes to update variables when dealing with large deformations. Further, our formulation using rotation matrices is, we feel, more transparent than other treatments (see, e.g. ABAQUS, 1996), which, like ours, allow for arbitrarily large deformations.

We note also that the end-to-end effective stiffness of a length of rod made of a sequence of elements can be obtained from inverting the effective *compliance*, for which there is a simple composition rule detailed in Appendix B. While this rule is completely equivalent to the commonly used method of static condensation (see, e.g. McGuire and Gallagher, 1979), it is more direct and easy to use due to its recursive nature.

Concatenating the changes in position and orientation at each node into a single column vector, say x, the quadratic minimization problem we have is to minimize the incremental total energy

$$\delta E^{\mathrm{tot}} = \frac{1}{2} x^T K x - L^T x, \tag{23}$$

subject to a linear constraint

$$Bx = b; \tag{24}$$

here, K is the total stiffness matrix for the system (catheter plus wall potential), b is a specified vector which constrains the displacements (for instance, b could be the position or orientation changes at the current node of insertion), and L is the total load vector. The linear constraint may be implemented by adding a Lagrange multiplier term $\lambda^T(Bx-b)$ to δE^{tot} above. It typically incorporates the condition that at the catheter's insertion point, it is translated and rotated by specified increments; this serves to determine six rigid degrees of freedom. The minimum of Eq. (23) subject to Eq. (24) may be found by solving the linear system (Lawton et al., 1997)

$$\begin{pmatrix} K & B^T \\ B & 0 \end{pmatrix} \begin{pmatrix} x \\ \lambda \end{pmatrix} = \begin{pmatrix} L \\ b \end{pmatrix}. \tag{25}$$

The Lagrange multiplier λ is the constraint force physically required to satisfy the linear constraint $Bx = b$. In the case when a single node is fixed and b is zero, alternatively, the constraint may be incorporated by simply leaving out from the linear system $Kx = L$ the appropriate six degrees of freedom in x and their corresponding 6×6 contribution to the stiffness K and their 6×1 contribution to the

load vector L; then the Lagrange multiplier λ is not required. We shall discuss simulation details in Section 5.

5. Numerical simulation and results

In general, the catheter, as it moves inside the arterial network, contacts the arterial wall at several places. Suppose that at time step t, the catheter makes contact with the wall at some set of nodal points, m in number, indexed by j with $j = 1,2,..., m$. The physician's manipulation at the point of insertion results in incremental displacements (changes in position and orientation) at the node of insertion, at time $(t + 1)$; we assume that these displacements are given as inputs. The catheter then simultaneously assumes some equilibrium configuration inside the arteries, and the nodes are accordingly displaced with respect to their earlier positions. As stated earlier, this requires the reasonable assumption that the catheter reaches an equilibrium within the time scale associated with a typical incremental displacement. The problem is then to determine such an equilibrium. For this, we need to make an initial estimate for the catheter's configuration at time $(t + 1)$, and then refine this estimate.

Our method of solution is therefore divided into two parts: first, a *placement method* makes a reasonable guess for the new catheter configuration, and second, a *relaxation* process finds an equilibrium by incremental energy minimization as discussed in the previous section. Given a small incremental displacement at the insertion node and a reasonable placement procedure, the catheter would remain close to an energy minimum, which makes this method feasible.

A natural method of placement is to assume that each contacting node slides along the wall in a direction tangential to the wall at that node; this is physically reasonable for a catheter (straight in its reference configuration) contacting a rigid frictionless straight wall. While we shall not consider friction here, we note that the curvature of the artery makes it essential to follow the placement step with the relaxation step. When there are no nodes on the catheter which contact the wall, the nodes are just rigidly displaced in the placement step. We shall now describe this tangential placement method in more detail.

Consider a node j which contacts the arterial wall. Tangential placement then means that the incremental displacement $\delta\mathbf{x}_j$ of this node is constrained, and may be written in the form

$$\delta\mathbf{x}_j = a_j\mathbf{u}_j + b_j\mathbf{v}_j, \tag{26}$$

where $\mathbf{u}_j$ and $\mathbf{v}_j$ are (arbitrary, but known) orthogonal unit vectors in the plane tangent to the wall at the contact point. Orientations are not constrained, and neither are the incremental displacements at non-contacting nodes. The six degrees of freedom at a contacting node j are thus written as linear combinations of the variables a_j, b_j and the orientation increments (a total of five degrees of freedom); denote the corresponding 6×5 matrix by A_j. At nodes which are inside the artery, the independent variables are directly the incremental changes in position and orientation. If there are a total of n catheter nodes, the independent variables are $(6n-m)$ in number; concatenate these into a vector y. If x is the concatenated vector of all $6n$ degrees of freedom, we may write

$$x = Ay, \tag{27}$$

where A is block diagonal with 6×5 sub-blocks A_j corresponding to contacting nodes j and 6×6 identity sub-blocks corresponding to non-contacting nodes.

Given an incremental manipulation by a physician at the inserted node, the tangential placement method *estimates* the new catheter configuration by minimizing the catheter's incremental elastic energy

$$\delta E_{\mathrm{el}} = \frac{1}{2} x^T K x = \frac{1}{2} y^T (A^T K A) y, \tag{28}$$

subject to the specified incremental displacements at the insertion node. We shall write $y = \binom{y_1}{y_2}$, where y_1 is the vector of six degrees of freedom at the insertion node, corresponding to translation and rotation increments there, and y_2 are all the other degrees of freedom. Note that $y_1 = x_1$ is given.

The size of the matrix K may be reduced by using the compliance rule given in Appendix B, so that we need to use only the effective stiffnesses of lengths of catheter between nodes contacting the arterial wall in order to build K.

Writing $\bar{K} = A^T K A$ in the form

$$\bar{K} = \begin{pmatrix} \bar{K}_{11} & \bar{K}_{12} \\ \bar{K}_{21} & \bar{K}_{22} \end{pmatrix}, \tag{29}$$

with $\bar{K}_{21} = \bar{K}_{12}^T$, the above minimization yields the solution

$$y_2 = -\bar{K}_{22}^{-1} \bar{K}_{21} y_1, \tag{30}$$

which determines the incremental changes in position and orientation at all the other nodes through the use of Eq. (27).

Now that we have an initial estimate of the catheter's actual updated configuration in terms of the increments x, a true equilibrium may be found by a process of relaxation. Thus, the linear system Eq. (25) may be iterated with these increments x as an initial guess until an equilibrium configuration is reached. This configuration is the shape taken by the catheter due to incremental insertion by the physician/user. In practice the iterative process of energy minimization is stopped when the load becomes small enough; this usually requires only very few cycles.

As a test case, we show results of inserting a catheter with a pigtail-shaped head, also called a pig-head catheter, into a Y-shaped tube. The length of the catheter is 10 units, and the radius of the Y-tube is *1* unit. In Fig. 4, the catheter is seen to be touching the interior surface of the Y-shaped tube. The catheter is then pushed in by 0.25 distance units, successively. The placement step in this case rigidly displaces the catheter. As a result, part of the catheter is seen to be lying outside the Y-tube. The result of relaxation brings the catheter to a minimum energy state, where the catheter is seen inside the wall. A succession of three placement–relaxation steps, starting from the initial configuration in Fig. 4, is shown in Fig. 5.

The effect of applied twist on the catheter inside the tube is depicted in Fig. 6, which shows the catheter shape as a result of twisting the catheter in steps of 0.5 radians about a vertical axis passing

Fig. 4. Initial configuration.

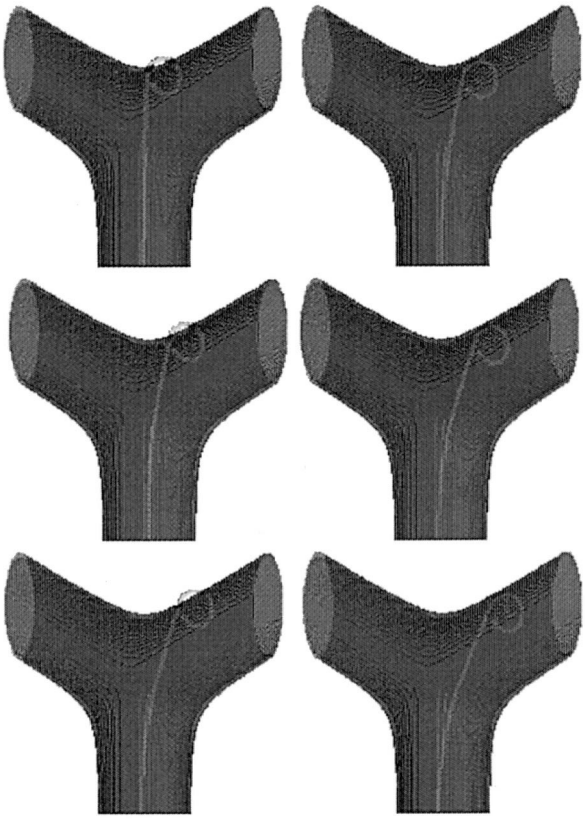

Fig. 5. Three pairs of successive placement–relaxation steps, from top to bottom.

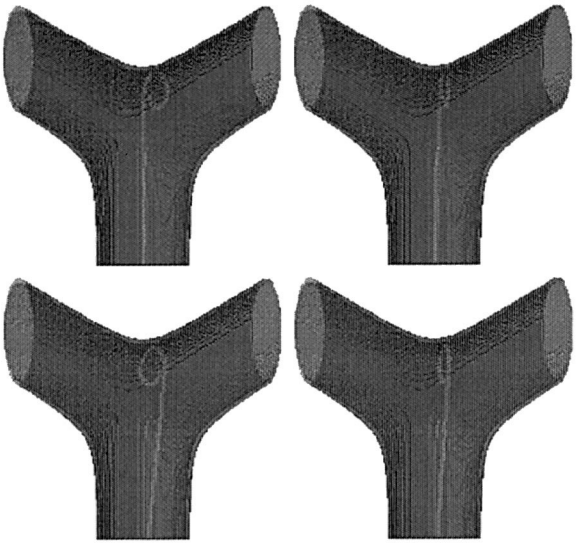

Fig. 6. An illustration of the effects of successive twisting, clockwise from top left.

through the bottom of the figure, starting from the configuration of Fig. 4. Only the end result after placement and relaxation is shown in each frame. It is evident that the combined effect of the applied twist and the confinement constraint produces torsion in the catheter configuration.

The maneuverability of the catheter is demonstrated in Fig. 7, which shows the catheter shape as a result of maneuvering starting from the catheter position in Fig. 4. It is not possible to move the catheter to the left branch of the Y-tube from the configuration of Fig. 4 by pushing alone. However a suitable combination of retraction, twisting, and pushing of the catheter can often help navigate a catheter to appropriate regions of choice. Thus, starting from the configuration in Fig. 4, a retraction of 0.3 units, and a twist of 2 radians, followed by pushing of the catheter shows the catheter getting into the left branch of the Y-tube.

In the next section, we describe our software simulator for catheter navigation, *da Vinci*, and present pictures of catheter–arterial wall interaction (with arterial data taken from human cadavers).

6. The *da Vinci* system

Interventional radiologists usually train on animals, or on a human patient under an expert's supervision. Catheters are not visible unless radio-opaque contrast agents are introduced. Excessive use of these agents, which can occur during training, may result in hazardous reactions for the patient, due to toxicity. In this context, simulators can significantly facilitate the training process.

The *da Vinci* system is a real-time, augmented reality-based training simulator for interventional radiology procedures with a 'virtual patient' (Anderson and Raghavan, 1997). In particular, it is designed to reproduce the 'look and feel' of a catheter lab and allows for choice from a range of catheter geometries and their physical properties. Different datasets may be incorporated into the system for experimentation with the navigation procedure. In such a procedure, the catheter is inserted into blood vessels through a sheath introduced by a puncture through the skin. The point of insertion and the angle of insertion (with respect to the arterial centreline) in a specified plane may be chosen by the user. Together with its advanced 3D-visualization capabilities, and a reasonably accurate physical model

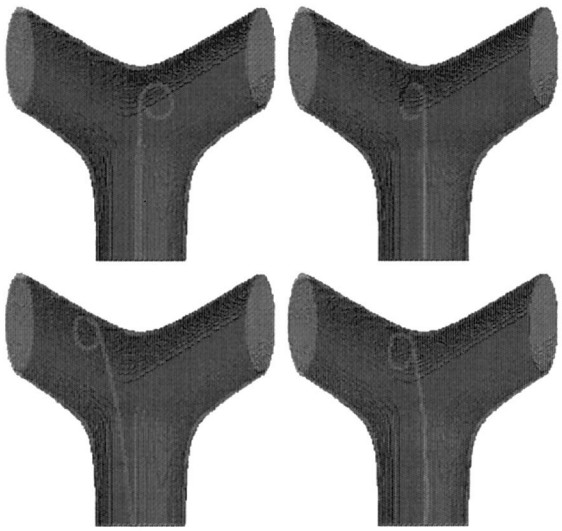

Fig. 7. Navigation by maneuvering of the catheter: retraction, twisting, and two push moves, shown clockwise from top left.

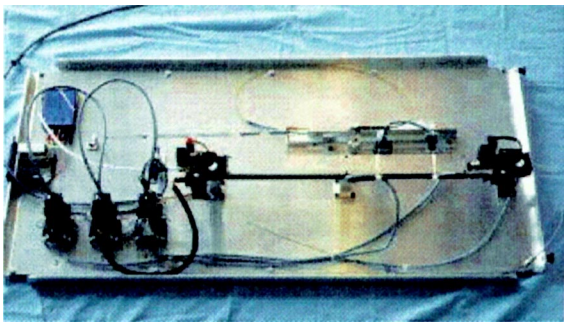

Fig. 8. A picture of the catheter input device hardware.

of catheter interaction with the arterial walls as described in this paper, the software is envisaged to provide training with a quality close to training on a real patient. The software can also be used by experts for pre-treatment planning.

In addition to the software system, a hardware input device which uses a real catheter and measures displacement and twist inputs at the point of insertion has been developed in collaboration with Loral

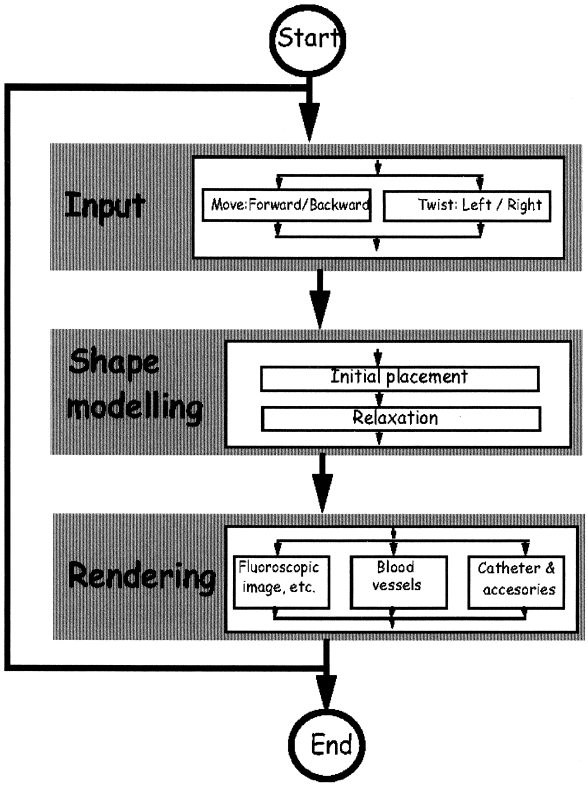

Fig. 9. System architecture.

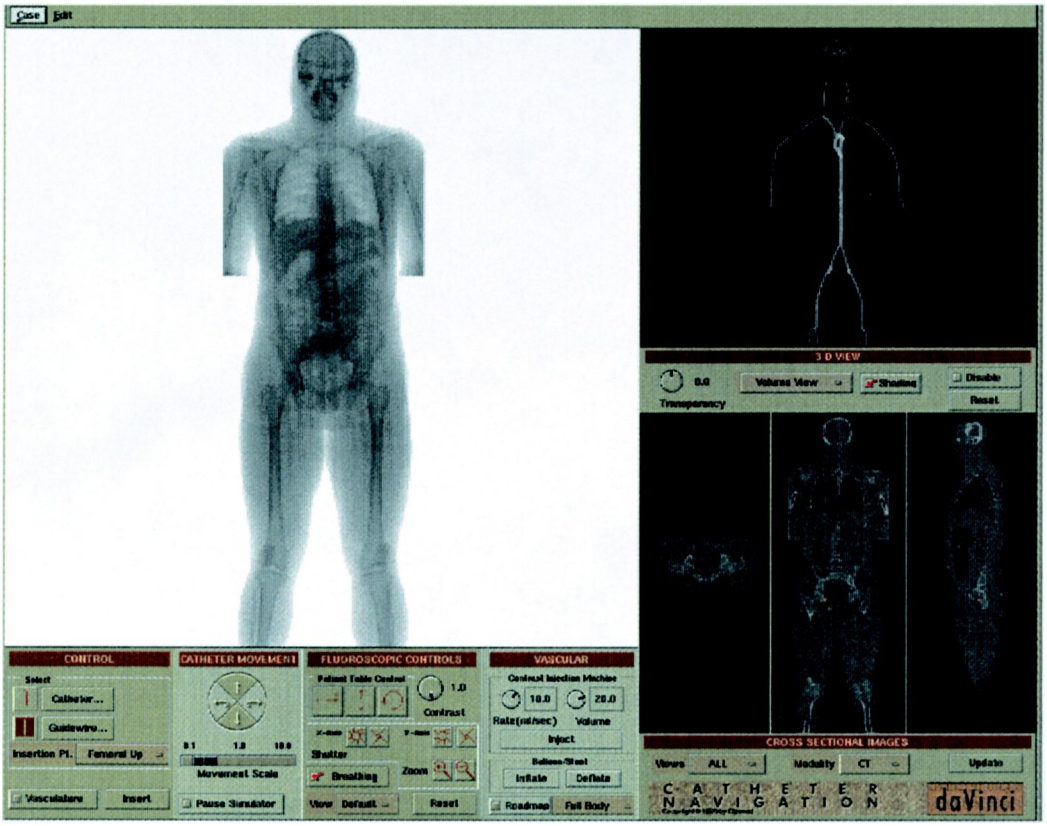

Fig. 10. An image of the system interface showing various controls and views (fluoroscopic, vascular tree, and slices).

Incorporated. Fig. 8 is an illustration of this device. The use of a real catheter significantly enhances the realism of the simulation training environment and adds to physician comfort.

The basic architecture of *da Vinci* is shown in Fig. 9. It consists of three modules: the input module, the shape modeling module, and the visualization module. The input module provides methods needed for user interaction with the system. It includes the process of selection of patient vasculature data, selection of type of catheter and guidewire, performing push/pull/twist operations, and choosing from a range of visualization tools. The heart of the system is the shape modeling module, the details of which have been discussed in earlier sections.

The visualization module provides methods for displaying the catheter along with the vasculature, so as to assist the user in navigation. It includes a two dimensional fluoroscopic image of the anatomy which shows the catheter configuration superimposed on the vasculature, as well as an advanced volume rendered image depicting the three dimensional morphology of the arterial structure along with the catheter. The user can choose the angle of view, the position of the 'patient' on the table, and the scale from a choice of interface buttons, using inputs from a computer mouse. In addition, the system can relate the catheter tip position with images of the surrounding anatomy in multiple planes (coronal, sagittal, axial). The three dimensional view and the multiplanar views are useful teaching aids during training.

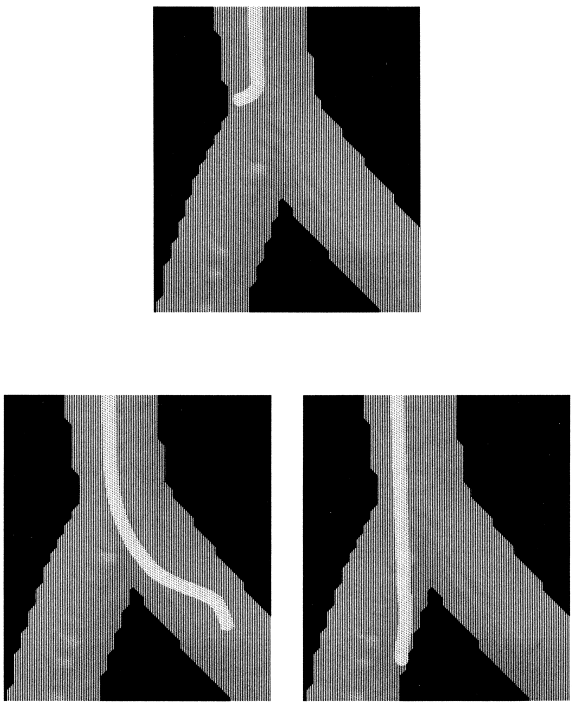

Fig. 11. Close-up views of a catheter before it enters an arterial branch (top), navigated into different legs of the branch (bottom).

Fig. 10, taken from our software system, depicts the user interface with various controls, which includes a fluoroscopic view and various sectional slices, as well as a model of the vascular tree. The top image in Fig. 11 shows a catheter just before it enters an arterial branch. The bottom images there show the catheter pushed into different legs of the branch by means of appropriate twisting operations. The interaction of the catheter with the artery wall may be observed in all of these images taken from the *da Vinci* system. The user-friendly, interactive nature of the system makes it a valuable environment for the design of catheters and other interventional devices, which, as mentioned earlier, is an important application.

In summary, we have detailed here the construction of a physical model for the efficient modeling and computation of catheter–blood vessel interaction, which forms the core of a simulation system designed for use in interventional radiology applications. We are working on the inclusion of devices such as balloons and stents in the model, as well as the incorporation of flexibility of the vessel walls. Further downstream, the modeling of hemodynamic effects will bring the system still closer to a good approximation to reality.

Acknowledgements

The software design and architecture of the *da Vinci* system was developed by H.T. Nguyen and Rakesh Mullick. We are grateful to Professor Jim Anderson for guidance on system requirements for realism in the clinical context.

Appendix A. Continuum thin rod elasticity

Intuitively, a thin rod is an object that admits a class of physical embeddings into space characterized by two properties: to each embedding there exists a parameterized *central curve* that describes the location of a center for a normal section; for each pair of embeddings, the correspondence between material points is *approximated* by a *deformation* that maps normal planes isometrically onto normal planes. We define the concept of a framed path or *ribbon* as the analogue of an orthonormal coordinate system to parametrize material points. It is easy to show that the set of deformations form an infinite dimensional Lie group that acts transitively on equivalence classes of embeddings called *configurations*. Bending and twisting of deformed thin rods are described using the associated Lie algebra.

Although we can extend the treatment to rods with corners (Lawton et al., 1999), we will not consider this case here.

Let R denote the real numbers and let R^3 denote three-dimensional Euclidean space. We define a physical thin rod having a rest length L (with arc length parameter $s \in [0,L]$) as a set of points B with a *physical embedding* (a one-to-one mapping)

$$f: B \rightarrow R^3,$$

and an associated central curve

$$\mathbf{r}: [0,L] \rightarrow R^3,$$

whose image $\mathbf{r}([0,L])$ is close to $f(B)$. We do not require that $f(B)$ contain the image of the central curve; for instance catheters are usually constructed as hollow tubes. Based on physical considerations, we shall restrict our family of thin tube deformations further to require that the deformation derivatives map normal planes (planes normal to the central curve) into normal planes. This model is a particular case of the special Cosserat theory (Antman, 1995) with one of the directors chosen to lie along the unit tangent to the centerline. That our restriction is a reasonable one may be seen by examining the reduction from three dimensional linear elasticity to one dimensional rod theories. This reduction is discussed in Lawton et al. (1999), where it is shown that one can think of rod theories as arising from an expansion in d/L, where d is the cross-sectional size and L is the length of the rod. In the limit of small d/L, a description in terms of normal planes alone may be seen to be an accurate one. Accordingly, we proceed with our treatment.

Let $SO(3)$ denote the rotation group on R^3. With respect to a basis for R^3, elements of $SO(3)$ are as usual represented by orthogonal 3×3 matrices with unit determinant.

We define a deformation $d = (\mathbf{a}, \alpha, M)$ to consist of

- a translation vector $\mathbf{a} \in R^3$,
- a bounded real function α, and
- a function $M(s)$: $[0,L] \rightarrow SO(3)$ whose derivative is square integrable.

Let $\mathscr{D}$ denote the set of deformations. It is straightforward to show that the set $\mathscr{D}$ forms an infinite dimensional Lie group under the product $(\mathbf{a}_1,\alpha_1,M_1)(\mathbf{a}_2,\alpha_2,M_2) \equiv (\mathbf{a}_1 + \mathbf{a}_2, \alpha_1 + \alpha_2, M_1 M_2)$, where addition and multiplication are performed pointwise. Furthermore, $\mathscr{D}$ acts as a group of transformations on the set of ribbons as follows: for a ribbon $(\mathbf{r},\mathbf{n})$ with unit tangent $\mathbf{r}' = \mathrm{d}\mathbf{r}/\mathrm{d}s$, and deformation $d = (\mathbf{a},\alpha,M)$ results in

$$d(\mathbf{r})(s) = \mathbf{r}(0) + \mathbf{a} + \int_0^s \mathrm{e}^{\alpha(\tau)} M(\tau)\mathbf{r}'(\tau)\mathrm{d}\tau \tag{31}$$

and

$$d(\mathbf{n})(s) = M(s)\mathbf{n}(s). \tag{32}$$

It is clear that for small $\alpha(s)$, this function can be given the interpretation of a local stretch rate along the rod. The rotation matrix $M(s)$ rotates the local frame defining the tangent and the normal plane to a corresponding new frame in the deformed rod; it is the assumption that normal planes are deformed to normal planes that allows us to parametrize the deformations in this manner. Here and henceforth we shall use a prime to denote a derivative with respect to s.

Associated with the rotation matrix $M(s)$ is the rotation rate $\omega(s) = M^T(s)M'(s)$. The matrix $\omega(s)$ is skewsymmetric and lies in the Lie algebra of $SO(3)$. Given a skewsymmetric 3×3 matrix,

$$\Omega = \begin{pmatrix} 0 & -\omega_3 & \omega_2 \\ \omega_3 & 0 & -\omega_1 \\ -\omega_2 & \omega_1 & 0 \end{pmatrix},$$

we may construct from it a vector $\boldsymbol{\omega}$ with components ω_1, ω_2 and ω_3. Generally, we shall denote by a boldface lower case letter the vector associated with the corresponding skewsymmetric matrix (denoted by the corresponding upper case letter), and vice versa.

Rotational and translational invariance dictates that the elastic energy density associated with a deformation must depend only on the vector function $\boldsymbol{\omega}$ and on the function α which measures the rate of longitudinal stretching. Furthermore, in the case of homogeneous and isotropic linearly elastic material, it may be shown (Lawton et al., 1999) that there is no coupling between stretch rate and rotation rate. In linear elasticity the energy density is a quadratic function in the stretch and rotation rate, so that we may write

$$J_{\mathrm{el}}(\alpha,\boldsymbol{\omega},s) = a\alpha^2 + \frac{1}{2}\boldsymbol{\omega} \cdot Q\boldsymbol{\omega}, \tag{33}$$

where $a > 0$ is a stretch modulus and the matrix Q is a generalized positive definite stiffness density. In particular, for a rod with circularly symmetric section, it may be shown that (Lawton et al., 1999; Landau and Lifshitz, 1970):

$$J_{\mathrm{el}}(\alpha,\omega,s) = \frac{E_{\mathrm{Y}}A}{2}\alpha^2 + \frac{G_{\mathrm{S}}J}{2}T^2 + \frac{E_{\mathrm{Y}}I}{2}B^2. \tag{34}$$

Here, T and B denote the magnitude of the twisting and bending components of the rotation rate $\boldsymbol{\omega}$ (measured with respect to the reference configuration which is assumed to be an elastic energy minimum). Let $\mathbf{u}$ denote the unit tangent along the reference configuration of the rod. Then the twist and bend vectors respectively are $\mathbf{T} \equiv (\boldsymbol{\omega}\cdot\mathbf{u})\mathbf{u}$ and $\mathbf{B} \equiv \boldsymbol{\omega} - (\boldsymbol{\omega}\cdot\mathbf{u})\mathbf{u}$. Here, E_{Y} is Young's modulus, G_{S} is the shear modulus, A is the cross sectional area, I is the second moment of area and $J = 2I$. Note that α, $\boldsymbol{\omega}$, T, B, A, I and the elasticity coefficients, E_{Y} and G_{S}, are in general functions of $s \in [0,L]$.

It is much easier for thin rods to bend and twist than it is for them to stretch. Consequently, the stretch term may be safely ignored in many situations and the elastic energy density is well-approximated by the last two terms in Eq. (34), which depend only on the rotation rate $\boldsymbol{\omega}$. We shall now derive equations describing equilibrium configurations with this assumption of zero stretch; the generalization to non-zero stretch is straightforward.

Let $\mathbf{r}_0(s)$ be the central curve of the thin rod in its reference configuration and let $\mathbf{u}(s)$ be the corresponding unit tangent. The position vector of a point at length s along the deformed thin rod is given from Eq. (31) as

$$\mathbf{r}(s) = \mathbf{r}_0(0) + \mathbf{a} + \int_0^s M(t)\mathbf{u}(t)\mathrm{d}t, \tag{35}$$

where $\mathbf{a}$ is a rigid translation. This relationship may be re-written in differential form as

$$\mathbf{r}'(s) = M(s)\mathbf{u}(s), \tag{36}$$

where the prime indicates differentiation with respect to s.

Recall also that the change of the rotation matrix M along the rod is

$$M'(s) = M(s)\Omega_M(s), \tag{37}$$

where $\Omega_M(s)$ is the instantaneous rotation rate of $M(s)$. Equilibrium configurations correspond to a minimum of the elastic energy, subject to the constraints of Eqs. (36) and (37), under the action of applied forces and torques.

We shall first consider the case where external forces arise through an interaction with a specified *potential field*. An equilibrium configuration of the thin rod is therefore one which is a stationary state for the following *augmented* energy functional:

$$H = \int_0^L \mathrm{d}s\left(\frac{1}{2}\boldsymbol{\omega}\cdot Q\boldsymbol{\omega} + J_{\mathrm{ex}}(\mathbf{r},s) + \boldsymbol{\lambda}\cdot(\mathbf{r}' - M\mathbf{u}) + \boldsymbol{\mu}\cdot(\boldsymbol{\omega}_M - \boldsymbol{\omega})\right). \tag{38}$$

We have introduced here the vectors $\boldsymbol{\lambda}(s)$ and $\boldsymbol{\mu}(s)$ which are Lagrange multiplier auxiliary variables which serve to enforce Eqs. (36) and (37). The dots between vectors indicate scalar products.

The problem of finding the equilibrium configuration of the thin rod is now recast as a constrained optimization problem. We seek a variational solution of this problem. The Euler–Lagrange variational equations we obtain will make the connection between applied forces and deformations. It is important to note that due to the nature of the variables, some variations are constrained. Variations of the rotation matrix M must be constrained such that upon a variation, the new rotation matrix remains a rotation. This means that a variation δM must take the form $M\delta A$, where δA is skewsymmetric (this restriction follows from the fact that $M^TM = I$).

Variational equations arising due to variations in $\boldsymbol{\lambda}$ and $\boldsymbol{\mu}$ yield the constraints (Eqs. (36) and (37)), as desired.

The variation in H due to a variation in $\boldsymbol{\omega}$ yields

$$\boldsymbol{\mu} - \frac{\partial J_{\mathrm{el}}}{\partial \boldsymbol{\omega}} = 0 \tag{39}$$

as the strong equation for stationarity.

A variation in $\mathbf{r}$ holding $\mathbf{r}(0)$ fixed yields the variational equation

$$\boldsymbol{\lambda}' = \frac{\partial J_{\mathrm{ex}}}{\partial \mathbf{r}}. \tag{40}$$

The variation in H due to a variation in M ($\delta M = M\delta A$, as mentioned above) may be shown to give the equation for stationarity

$$\boldsymbol{\mu}' = \boldsymbol{\mu}\times\boldsymbol{\omega} + (M^T\boldsymbol{\lambda}\times\mathbf{u}). \tag{41}$$

It is possible to rewrite this equation in a more elegant form by defining a new variable $\boldsymbol{\xi}(s) \equiv M(s)\boldsymbol{\mu}(s)$. Using the above equation Eq. (41) for the rate of change of $\boldsymbol{\mu}$, it is easy to see that the rate of change of $\boldsymbol{\xi}$ along the rod is given by

$$\boldsymbol{\xi}' = \boldsymbol{\lambda} \times (M\mathbf{u}) = \boldsymbol{\lambda} \times \mathbf{r}'. \tag{42}$$

It may be seen by integrating Eqs. (40) and (42) by parts that $\boldsymbol{\lambda}(s)$ and $\boldsymbol{\xi}(s)$ have the interpretations of internal force and internal torque respectively, on a normal section at arc length parameter s. Since J_{el} is quadratic in $\boldsymbol{\omega}$, we may use Eq. (39) to write

$$\boldsymbol{\xi} = MQ\boldsymbol{\omega}. \tag{43}$$

In the presence of both an external potential energy density J_{ex} giving rise to a force density, and an external torque density $\boldsymbol{\tau}'$, the equations describing a thin rod equilibrium configuration take the form

$$\mathbf{r}' = M\mathbf{u},$$

$$M' = M\Omega,$$

$$\boldsymbol{\lambda}' = \frac{\partial J_{\mathrm{ex}}}{\partial \mathbf{r}}$$

and

$$(Q\boldsymbol{\omega})' = \left[(M^T\boldsymbol{\lambda}) \times \mathbf{u}_0 - \boldsymbol{\omega} \times Q\boldsymbol{\omega} + M^T\boldsymbol{\tau}'\right]. \tag{44}$$

These equations must be supplemented with appropriate boundary conditions, which can take several forms depending on whether the ends are free or forced. As an example, the position $\mathbf{r}(0)$ and orientation $M(0)$ may be specified at one end $s = 0$, while the applied force and moment, $\boldsymbol{\lambda}(L)$ and $\boldsymbol{\xi}(L) = MQ\boldsymbol{\omega}(L)$ respectively, might be specified at the other end $s = L$.

In general, these equations with their boundary conditions determine a two-point boundary value problem. Shooting methods may be used to find solutions of these highly non-linear equations. These methods are particularly simple to implement for the case of incremental loading, for which perturbative solutions are discussed in Lawton et al. (1999).

Appendix B. Compliance and its composition

Here, we shall provide a rule to compute the compliance of a sequence of thin rod segments connected by stiff joints, by recursively composing the compliances of pairs of adjacent segments. Besides being useful in computing the effective compliance (and thus the effective stiffness) of long lengths of catheter, it is of use when dealing with objects such as partially constrained robotic arms and protein molecules, whose segments exhibit constrained deformations. The compliance expresses the incremental deformation of a thin rod configuration as a linear function of external force increments.

While the rule below is equivalent to the well-known procedure of static condensation commonly found in the structural analysis literature (see, e.g. McGuire and Gallagher, 1979), the novel composition of compliances we obtain for a sequence of thin rod segments is more direct and computationally very efficient.

For a finite length of rod of arbitrary shape, the force–displacement relationship when one end of a rod is held fixed and the other (free) end is displaced may be expressed in terms of the associated stiffness matrix K for the rod:

$$\begin{pmatrix} \delta\mathbf{F} \\ \delta\boldsymbol{\tau} \end{pmatrix} = K \begin{pmatrix} \delta\mathbf{r} \\ \delta\boldsymbol{\theta} \end{pmatrix}, \tag{45}$$

where the 6×6 matrix K relates small changes in position and orientation at the free endpoint to an applied force and torque (both small) there. When both endpoints move (as would happen in general when the rod is part of a larger segment), the above relation still holds, with $\delta\mathbf{r}$ and $\delta\boldsymbol{\theta}$ now quantifying the strain, or deviation from rigidity, of the rod.

The inverse form of this relationship is given by a *compliance* matrix C ($C = K^{-1}$ when K is well-conditioned), which describes the linear response of the rod to small applied forces and torques; thus, the compliance C is defined by the equation

$$\begin{pmatrix} \delta\mathbf{r} \\ \delta\boldsymbol{\theta} \end{pmatrix} = C \begin{pmatrix} \delta\mathbf{F} \\ \delta\boldsymbol{\tau} \end{pmatrix}. \tag{46}$$

In cases where displacements of the free end are constrained by a reduced set of degrees of freedom (due to very large stiffnesses of some kinds of displacements relative to others, for instance), or when the incremental displacements of a long rod segment (composed of a series of smaller ones) forced only at its endpoints need to be determined, it is useful to work with the compliance matrix. The former case arises in the modeling of protein deformations, where the degrees of freedom are tightly constrained by the nature of the chemical bonds linking backbone atoms; in such a case the compliance matrix C is well-defined, but is not invertible. The latter case arises in catheter navigation simulation where the catheter often makes contact with the arterial walls only at a discrete set of points.

When a rod consists of a sequence of segments connected by stiff joints, an *effective* compliance describes the linear response of the free end. Specifically, consider the case where a rod consists of two parts $a = (\mathbf{x}_1, \mathbf{x}_2)$ and $b = (\mathbf{x}_2, \mathbf{x}_3)$, with $\mathbf{v}_a = \mathbf{x}_2 - \mathbf{x}_1$ and $\mathbf{v}_b = \mathbf{x}_3 - \mathbf{x}_2$, and with corresponding compliance matrices C_a and C_b (see Fig. 12). Suppose now that a small force–torque pair $(\delta\mathbf{F}, \delta\boldsymbol{\tau})$ is applied at the end $\mathbf{x}_3$ of rod b, with $\mathbf{x}_1$ held fixed.

For rod a, there is a net force $\delta\mathbf{F}$ and a net torque $\delta\boldsymbol{\tau}_{\text{net}} = (\delta\boldsymbol{\tau} + \mathbf{v}_b \times \delta\mathbf{F})$ acting at the endpoint $\mathbf{x}_2$. The end $\mathbf{x}_1$ is fixed; therefore, the strain of rod a is $(\delta\mathbf{x}_a, \delta\boldsymbol{\theta}_a) = (\delta\mathbf{x}_2, \delta\boldsymbol{\theta}_2)$. Consequently, we have the relation

$$\begin{pmatrix} \delta\mathbf{x}_2 \\ \delta\boldsymbol{\theta}_2 \end{pmatrix} = C_a \begin{pmatrix} I & 0 \\ V_b & I \end{pmatrix} \begin{pmatrix} \delta\mathbf{F} \\ \delta\boldsymbol{\tau} \end{pmatrix}, \tag{47}$$

where I is the 3×3 identity matrix and V_b is the skewsymmetric matrix corresponding to $\mathbf{v}_b$.

For rod b, it is clear that the deviation from rigidity, or strain, has position and orientation components matrix

$$\delta\mathbf{x}_b = \delta\mathbf{x}_3 - (\delta\mathbf{x}_2 + \delta\boldsymbol{\theta}_2 \times \mathbf{v}_b)$$

and

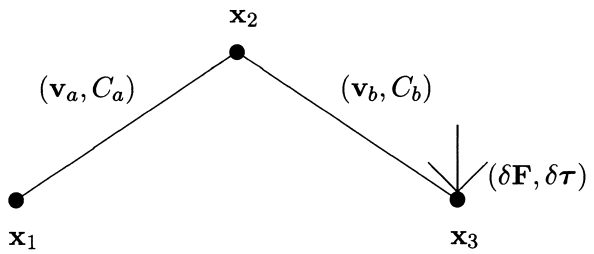

Fig. 12. Compliance composition for two segments connected by a stiff joint.

$$\delta\boldsymbol{\theta}_b = \boldsymbol{\theta}_3 - \boldsymbol{\theta}_2, \tag{48}$$

respectively; thus these components are zero if the rod undergoes a purely rigid motion.

Using Eq. (48) and Eq. (47) above, the relation

$$\begin{pmatrix} \delta\mathbf{x}_b \\ \delta\boldsymbol{\theta}_b \end{pmatrix} = C_b \begin{pmatrix} \delta\mathbf{F} \\ \delta\boldsymbol{\tau} \end{pmatrix} \tag{49}$$

for rod b may be rewritten in the form

$$\begin{pmatrix} \delta\mathbf{x}_3 \\ \delta\boldsymbol{\theta}_3 \end{pmatrix} = C_{\text{eff}} \begin{pmatrix} \delta\mathbf{F} \\ \delta\boldsymbol{\tau} \end{pmatrix}. \tag{50}$$

The *composition rule* for compliances is thus:

$$C_{\text{eff}} = C_b + T_{\mathbf{v}_b} C_a T^T_{\mathbf{v}_b}. \tag{51}$$

Here, we have defined the matrix

$$T_{\mathbf{v}_b} \equiv \begin{pmatrix} I & -V_b \\ 0 & I \end{pmatrix}. \tag{52}$$

For a series of rods connected by stiff joints, Eq. (51) above may be recursively used to generate the effective compliance of the entire sequence. It is clear that the effective compliance, which dictates the linear response of the system, is dependent on the geometry of the current configuration, in addition to the material properties. Furthermore, the composition law Eq. (51) is non-commutative and corresponds to the composition rule for a twenty four dimensional non-commutative Lie group (each rod is described by a vector $\mathbf{v}_i$ and a 6×6 symmetric matrix C_i, for a total of 24 degrees of freedom).

As mentioned earlier, Eq. (51) for composition of compliances is also very useful in computing deformations of a sequence of rods with constrained degrees of freedom, as we shall discuss in a forthcoming paper where protein deformations are modeled.

References

ABAQUS, 1996. ABAQUS Manuals. Hibbitt, Karlsson and Sorensen Inc, Pawtucket, Rhode Island.

Anderson, J., Brody, W., Kriz, C.J., Wang, Y., Raghavan, R., Viswanathan, R., 1996. *da Vinci*: a vascular catheterization and interventional radiology-based training and patient pretreatment planning simulator. J. Vasc. Intervent. Radiol. 7 (Part 2), 373.

Anderson, J., Raghavan, R., 1997. Virtual reality in interventional radiology. Min. Invas. Ther. and Allied Technology 6, 111–116.

Antman, S.S., 1995. Nonlinear Problems in Elasticity. Springer–Verlag, Berlin.

Gilmore, R., 1974. Lie Groups, Lie Algebras and Some of Their Applications. John Wiley, New York.

Landau, L.D., Lifshitz, E.M., 1970. Theory of Elasticity. Pergamon Press, New York.

Lawton, W., Poston, T., Raghavan, R., Ranjan, S.R., Viswanathan, R., Wang, Y.P., Yu, Y., 1997. Variational methods in biomedical computing. In: Computational Science for the 21st Century. John Wiley, England.

Lawton, W., Raghavan, R., Ranjan, S.R., Viswanathan, R.R., 1999. Ribbons and groups: A thin rod theory for catheters and filaments. J. Phys. A 32 (9), 1709–1735.

Love, A.E.H., 1944. A Treatise on the Mathematical Theory of Elasticity. Dover Publications, New York.

McGuire, W., Gallagher, R.H., 1979. Matrix Structural Analysis. John Wiley & Sons, New York.

Rao, S.S., 1989. The Finite Element Method in Engineering. Pergamon Press, New York.

Simo, J.C., 1985. A finite strain beam formulation. The three-dimensional dynamic problem, Part I. Computer Methods in Applied Mechanics and Engg. 49, 55–70.

Simo, J.C., Vu-Quoc, L., 1986. A three-dimensional finite strain rod model, Part II: Computational aspects. Computer Methods in Applied Mechanics and Engg. 86, 79–116.

Sternberg, S., 1964. Lectures on Differential Geometry. Chelsea Publishing Company, New York.